Near-source error sensor strategies for active vibration isolation of machines

C.A.J. Beijers[1], **T.G.H. Basten**[2], **D.R. van den Brink**[2], **J.W. Verheij**[2], **A. de Boer**[1]
[1] University of Twente
P.O. Box 217, 7500 AE Enschede, The Netherlands
e-mail: **c.a.j.beijers@utwente.nl**

[2] TNO TPD, Sound and Vibration Division
P.O. Box 155, 2600 AD Delft, The Netherlands
e-mail: **basten@tpd.tno.nl**

Abstract
Due to lightweight construction of vehicles and ships, the reduction of structure borne interior noise problems with passive isolation of engine vibrations might be not sufficient. To improve the isolation, a combination of passive and active isolation techniques can be used (so-called hybrid isolation). This paper focusses on the influence of the sensor positions on the performance of the active isolation. In general two strategies can be distinguished: sensors located in the accommodation with a direct minimization of the sound field and sensors located near the source of vibration. In this paper attention will be paid to an effective weighting of the near-source sensors in such a way that the interior noise in the vehicle is reduced. Also the near-source strategy of minimization of the injected power is considered. The latter strategy is theoretically very attractive, but is much more difficult to implement in practice. The techniques are explained and compared to each other with the help of numerical models.

1 Introduction

Passive vibration isolators are commonly used for isolation of machinery in transport vehicles and ships. However, the tendency to design lighter carrier structures and the customer demands for more comfort requires additional efforts to reach a better isolation. The effect that can be reached by passive isolation is limited because the stiffness of the mounting support is constrained due to other design requirements. For improved vibration isolation, active isolation can be applied which is especially effective for very flexible and lightweight structures. A combination of passive and active isolation (so-called hybrid isolation) combines passive vibration isolators with relatively high stiffness in one or more directions with active isolation techniques.

In Figure 1 a schematic overview of a hybrid isolation system in a ship is depicted. The diesel engine (source of vibration) is supported by a mounting system containing hybrid mounts. These mounts consist of passive vibration isolators combined with electronically controlled actuators close to or integrated with the passive mounts. The actuators are driven by the controller which minimizes the error sensor signals. The vibrations of the diesel engine are transmitted through the mounts and cause vibrations of the hull of the ship (also called receiver structure) and interior noise in the accommodations of the ship. It is assumed that the noise is dominated by the structure-borne sound from the engine, with the largest contributions originating from the engine orders. The rotary machinery cause in fact a deterministic excitation and for this reason feedforward control strategies can be used to tackle the control problem.

An important issue concerning the effectiveness of the active isolation system is the location of the error

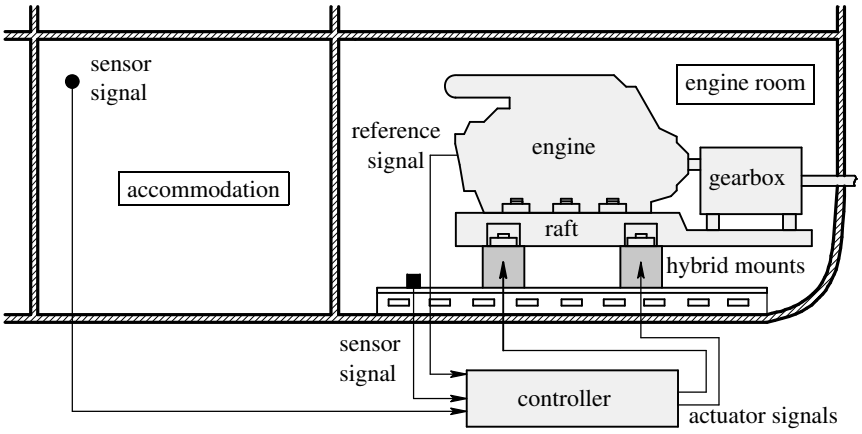

Figure 1: A schematic overview of a hybrid isolation system for a ship engine.

sensors. In Figure 1 the sensors are located at two different places. For instance microphones can be located in the accommodation itself and used as error sensors to reduce the measured sound field directly (so-called far-field sensors). This is an Active Structural Acoustic Control (ASAC) approach because the controller minimizes the interior sound fields measured by the microphones by influencing the structural behavior of the receiver structure with the actuators. Another option is to place error sensors (e.g. accelerometers) near the source of vibration (so-called near-source sensors). The advantage is that it is far more easy to implement (easier implementation and less wiring with respect to the sensors) and besides that, it may be possible to define a more global measure of the total sound field in the whole ship and a more global reduction can be achieved. The first approach will only result in a reduction of the sound field in the accommodation where the error sensors are placed, whereas in a accommodation elsewhere in the ship the noise level is not necessarily reduced.

Winberg, Johansson and Lagö showed that the first approach with use of far-field error microphones works quite well to reduce the noise in a passenger compartment in a boat at the first and second blade pass frequencies of the propeller and some engine orders. The results were obtained with simulations with measured transfer functions [1]. Using near-source error sensors at the mounts in one direction resulted in no reduction of the interior noise. Because of the multi-directional nature of the structure-borne sound transmission, the use of vibration transducers close to hybrid mounts (near-source sensors) has shown to give disappointing noise reductions in the accommodation. The vibrations are attenuated in the direction of the sensors, but still structure-borne sound is transmitted in the other directions. Also results of on board experiments with error microphones in the accommodation were presented [2].

This paper focusses on the use of near-source sensor strategies to achieve noise reduction in the far-field (e.g. accommodations in a ship). Two types of near-source sensor strategies are considered:

- minimization of the transmitted power to the receiver structure;
- weighting of the near-source vibration sensors based on responses of a set of well-chosen far-field sensors.

The first approach has already been studied in literature for simple receiver models, like e.g. Pan, Hansen and Pan [3].

First the theory is described to determine the passive and active response of the theoretical models of hybrid isolation systems. After that the different control strategies are analyzed and presented. The conditions for using a near-source sensor strategy based on weighting of the near-source sensor with a far-field approach are considered in more detail.

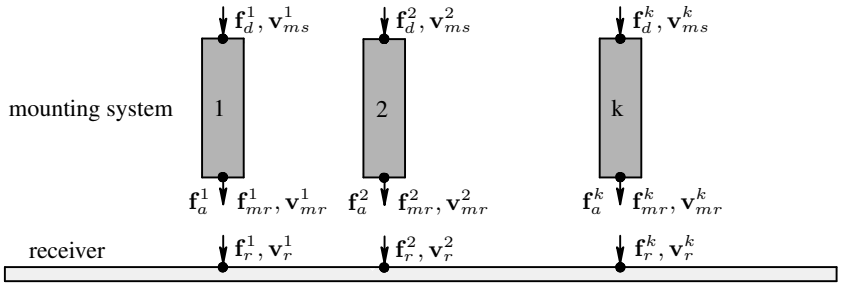

Figure 2: General model of a hybrid isolation system.

2 Theory: the dynamics

Considering hybrid isolation systems, in general three different components are analyzed: a source (the source of vibration, e.g. engine or a gearbox), a mounting support system and a receiver structure (like e.g. the vehicle or ship). In the approach presented in this paper, the source will be represented by a set of excitation forces on the top of the mounts. The dynamics of the whole hybrid isolation system is described by a mobility and impedance matrix approach at the different connection points (junctions) of the components. This type of approach allows an easy implementation of different models of the components (e.g. numerical or analytical models or even experimentally determined impedances of different mountings) and is adapted from a similar model presented by Gardonio, Elliott and Pinnington [4, 5].

2.1 Model description

In Figure 2 a complete model of a hybrid isolation system is depicted. Each vector (force and velocity) contains six components: three components in the translational directions and three components in the rotational directions. The total velocity vector $\mathbf{v}_{ms}$ and the total disturbance force vector $\mathbf{f}_d$ at the top or the source side of the mount force are written respectively as

$$\mathbf{v}_{ms} = \begin{Bmatrix} \mathbf{v}_{ms}^1 \\ \mathbf{v}_{ms}^2 \\ \vdots \\ \mathbf{v}_{ms}^k \end{Bmatrix} \qquad \mathbf{f}_d = \begin{Bmatrix} \mathbf{f}_d^1 \\ \mathbf{f}_d^2 \\ \vdots \\ \mathbf{f}_d^k \end{Bmatrix}, \tag{1}$$

where the number in the superscript represents the mount number. In the same way the other total velocity and force vectors are written as

$$\mathbf{v}_{mr} = \begin{Bmatrix} \mathbf{v}_{mr}^1 \\ \mathbf{v}_{mr}^2 \\ \vdots \\ \mathbf{v}_{mr}^k \end{Bmatrix} \qquad \mathbf{f}_{mr} = \begin{Bmatrix} \mathbf{f}_{mr}^1 \\ \mathbf{f}_{mr}^2 \\ \vdots \\ \mathbf{f}_{mr}^k \end{Bmatrix} \qquad \mathbf{v}_r = \begin{Bmatrix} \mathbf{v}_r^1 \\ \mathbf{v}_r^2 \\ \vdots \\ \mathbf{v}_r^k \end{Bmatrix} \qquad \mathbf{f}_r = \begin{Bmatrix} \mathbf{f}_r^1 \\ \mathbf{f}_r^2 \\ \vdots \\ \mathbf{f}_r^k \end{Bmatrix}, \tag{2}$$

where $\mathbf{v}_{mr}$ and $\mathbf{f}_{mr}$ the velocity and force vector at the receiver or bottom side of the mount respectively and $\mathbf{v}_r$ and $\mathbf{f}_r$ the velocity and force vector on the receiver structure.

The dynamics of the mounting system is described by impedance matrices according to [6]:

$$\mathbf{f}_d = \mathbf{Z}_{m11}\mathbf{v}_{ms} + \mathbf{Z}_{m12}\mathbf{v}_{mr} \tag{3}$$

$$\mathbf{f}_{mr} = \mathbf{Z}_{m21}\mathbf{v}_{ms} + \mathbf{Z}_{m22}\mathbf{v}_{mr} + \mathbf{T}_a\mathbf{f}_a, \tag{4}$$

where $\mathbf{Z}_{m11}$ and $\mathbf{Z}_{m22}$ are the blocked dynamic driving point impedance matrices at the top and bottom side of the mounting support respectively, $\mathbf{Z}_{m12}$ and $\mathbf{Z}_{m21}$ the blocked dynamic transfer impedance matrices of the mounting support, $\mathbf{T}_a$ a transformation matrix to define the degrees of freedom which are actuated and $\mathbf{f}_a$ the vector with actuator forces. The actuator forces are assumed to act at the bottom only of each mount as depicted in Figure 2. The dynamics of the receiver structure is determined with a mobility matrix approach according to

$$\mathbf{v}_r = \mathbf{Y}_r \mathbf{f}_r, \tag{5}$$

with $\mathbf{Y}_r$ the mobility matrix of the receiver structure. The dynamics of the total isolation system is determined by coupling the derived expressions of the dynamics of the components by demanding continuity for the velocity vectors and equilibrium for the force vectors at the junctions

$$\mathbf{T}\,\mathbf{f}_{mr} = -\mathbf{f}_r \qquad \mathbf{T}\,\mathbf{v}_{mr} = \mathbf{v}_r, \tag{6}$$

where $\mathbf{T}$ is a transformation matrix to transfer the local coordinate system, for which equation (3) is derived, to the coordinate system of the receiver structure. With help of the derived equations, all velocities and forces at the junctions of the total hybrid isolation system can be written as function of the disturbance force vector $\mathbf{f}_d$ and the actuator force vector $\mathbf{f}_a$

$$\mathbf{v}_{ms} = \left(\mathbf{Z}_{m11}^{-1} + \mathbf{Z}_{m11}^{-1}\mathbf{Z}_{m12}\mathbf{T}^{-1}\mathbf{Y}_r\mathbf{T}\mathbf{H}_1\right)\mathbf{f}_d + \left(\mathbf{Z}_{m11}^{-1}\mathbf{Z}_{m12}^{-1}\mathbf{T}^{-1}\mathbf{Y}_r\mathbf{T}\mathbf{H}_2\right)\mathbf{f}_a, \tag{7}$$

$$\mathbf{v}_{mr} = -\mathbf{T}^{-1}\mathbf{Y}_r\mathbf{T}\mathbf{H}_1\mathbf{f}_d - \mathbf{T}^{-1}\mathbf{Y}_r\mathbf{T}\mathbf{H}_2\mathbf{f}_a, \tag{8}$$

$$\mathbf{v}_r = -\mathbf{Y}_r\mathbf{T}\mathbf{H}_1\mathbf{f}_d - \mathbf{Y}_r\mathbf{T}\mathbf{H}_2\mathbf{f}_a, \tag{9}$$

$$\mathbf{f}_{mr} = \mathbf{H}_1\mathbf{f}_d + \mathbf{H}_2\mathbf{f}_a \tag{10}$$

$$\mathbf{f}_r = -\mathbf{T}\mathbf{H}_1\mathbf{f}_d - \mathbf{T}\mathbf{H}_2\mathbf{f}_a, \tag{11}$$

with

$$\mathbf{H}_1 = \left[\mathbf{I} - \left(\mathbf{Z}_{m21}\mathbf{Z}_{m11}^{-1}\mathbf{Z}_{m12} - \mathbf{Z}_{m22}\right)\mathbf{T}^{-1}\mathbf{Y}_r\mathbf{T}\right]^{-1}\mathbf{Z}_{m21}\mathbf{Z}_{m11}^{-1}, \tag{12}$$

$$\mathbf{H}_2 = \left[\mathbf{I} - \left(\mathbf{Z}_{m21}\mathbf{Z}_{m11}^{-1}\mathbf{Z}_{m12} - \mathbf{Z}_{m22}\right)\mathbf{T}^{-1}\mathbf{Y}_r\mathbf{T}\right]^{-1}\mathbf{T}_a. \tag{13}$$

2.2 Dynamics of mounting support

The dynamics of the mounting system is described by an impedance matrix formulation according to equations (3) and (4). The dynamic behavior is described with the velocity vector $\mathbf{v}_{ms}$ and the force vector $\mathbf{f}_d$ at the top of the mount and the velocity vector $\mathbf{v}_{mr}$ and the force vector $\mathbf{f}_{mr}$ at the bottom of the mount. In this way wave effects and non-rigid sources and receivers are taken into account when it is assumed that the velocities and forces are frequency dependent. In general rubber vibration isolators are used for passive isolation of the source. The impedance matrices of this kind of isolators can be determined experimentally or in a numerical way. It is noticed that the number of degrees of freedom for each end of the isolator is six, which implies that the size of the impedance matrices is $k \times 6$ by $k \times 6$, where k is the number of mounts. The transfer of structure-borne sound is a multidirectional phenomenon that is correctly described in this way. The impedance matrices can be determined in different ways, e.g. by measurements [7] or by numerical simulations [8]. In this paper models of four simple beams are used for which the impedance matrices are derived with the Finite Element package ANSYS. The actuators act in the axial direction of the bottom side of each mount, see Figure 2.

2.3 Dynamics of the receiver structure

Hybrid isolation systems for heavy machinery in vehicles have quite complex receiver structures. TNO TPD built a small-scale laboratory arrangement that, as a vibratory system, has sufficient complexity to offer

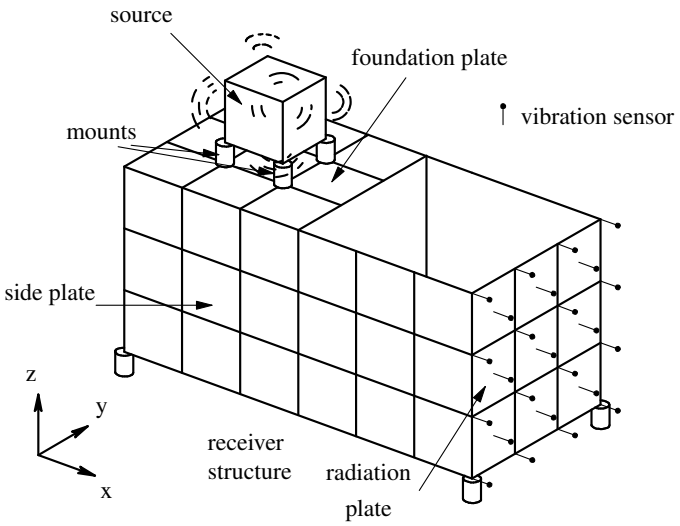

Figure 3: Sketch of the hybrid isolation model with far-field sensor set at TNO TPD.

some difficulties representative for a hybrid isolation system in a ship. It is shown in Figure 3. The test arrangement was designed to develop and test different active isolation strategies and as a demonstration setup for an operational hybrid isolation system. The test setup is simple enough to be modeled using numerical techniques like the finite element method. These numerical simulations are useful to analyze the influence of for example actuator and sensor positions and other physical properties on the performance of the hybrid isolation system. Earlier work on this laboratory arrangement related with actuator and sensor configurations has been published by Basten and Verheij [9].

For a fast computation of the different frequency response functions the receiver structure is modeled with the finite element package ANSYS to compute the eigenfrequencies and eigenmodes. The result of the finite element analysis is imported in MATLAB, where the different frequency response functions are computed, the isolation components (source, mounting system and receiver structure) are coupled with each other and the hybrid isolation response is calculated for the different defined sensor sets [10].

2.3.1 Equations of motion

For an undamped system the equation of motion which is composed and solved by the finite element package, is written as:

$$\mathbf{M}\ddot{\mathbf{u}} + \mathbf{K}\mathbf{u} = \mathbf{f} \tag{14}$$

with $\mathbf{M}$ the mass matrix (size $n \times n$), $\mathbf{K}$ the stiffness matrix (size $n \times n$), $\mathbf{f}$ the external force vector and $\mathbf{u}$ and $\ddot{\mathbf{u}}$ the vectors with the displacements and accelerations at all n degrees of freedom of the model respectively. With the assumption that the system is excited harmonically, the response can be expressed as $\mathbf{u}(t) = \mathbf{u}e^{j\omega t}$ (where $\mathbf{u}$ the amplitude of the displacement and ω the angular frequency) the homogeneous form of equation (14) results in an eigenvalue problem. Solving this equation results in the matrix $\mathbf{\Omega}$ which is a diagonal matrix with on the i^{th} location the natural frequency ω_i and the modal matrix $\mathbf{\Phi}$ which is a matrix with corresponding eigenmodes in each column. The modal matrix is normalized to the mass matrix. The solution of $\mathbf{u}$ for each frequency can now be written in the form of a modal superposition according to

$$\mathbf{u} = \mathbf{\Phi}\mathbf{q}, \tag{15}$$

where $\mathbf{q}$ the vector with modal participations. Substituting equation (15) in equation (14) and solving for the generalized coordinate $\mathbf{q}$ yields:

$$-\omega^2\mathbf{q} + \mathbf{\Omega}^2\mathbf{q} = \mathbf{\Phi}^{\mathrm{T}}\mathbf{f}\ , \tag{16}$$

where $(.)^{\mathrm{T}}$ indicates the transpose of the vector or matrix. In the receiver structure several damping mechanisms play a role: structural damping of the plate and beam material, damping caused by welds and connections and damping caused by interaction with the surrounding environment. The latter effect causes excitation of the air by the structural vibrations resulting in radiated sound power which is experienced as noise in the receiver structure. All these damping effects are taken into account with help of the definition with a structural damping coefficient (or loss factor) η. The equations of motion can subsequently be written as

$$-\omega^2\mathbf{q} + (1+\mathrm{j}\eta)\,\mathbf{\Omega}^2\mathbf{q} = \mathbf{\Phi}^{\mathrm{T}}\mathbf{f}\ . \tag{17}$$

2.3.2 Truncated modal expansion and residual flexibility

The derived equations of motion are determined without omitting information in the modal expansion. However, already a good estimate of the response in a certain frequency band is obtained when only modes with an eigenfrequency in or close to the frequency band of interest are taken into account. This truncation may lead to large errors, especially in driving point frequency response functions (like e.g. driving point mobilities). The accuracy of the modal expansion can be improved with the concept of residual flexibility [11]. The dynamic response in a frequency band $[0, \omega_b]$ is determined by substitution of the modal participations described by equation (17) into equation (15) according to

$$\mathbf{u} = \sum_{i=1}^{m} \boldsymbol{\phi}_i q_i + \sum_{i=m+1}^{n} \boldsymbol{\phi}_i q_i, \qquad q_i = \frac{\boldsymbol{\phi}_i^{\mathrm{T}}\mathbf{f}}{(1+\mathrm{j}\eta)\,\omega_i^2 - \omega^2}, \tag{18}$$

where q_i the i^{th} modal participation and $\boldsymbol{\phi}_i$ mode i. The modal expansion is truncated to m modes ($m \ll n$), so the error in prediction of the response $\mathbf{u}$ is described by the contribution of the modes $m+1$ to n. The maximum frequency of interest ω_b is much smaller than the eigenfrequencies for modes satisfying $i > m$ and the response can be approximated by

$$\mathbf{u} \approx \sum_{i=1}^{m} \frac{\boldsymbol{\phi}_i\boldsymbol{\phi}_i^{\mathrm{T}}\mathbf{f}}{(1+\mathrm{j}\eta)\,\omega_i^2 - \omega^2} + \sum_{i=m+1}^{n} \frac{\boldsymbol{\phi}_i\boldsymbol{\phi}_i^{\mathrm{T}}\mathbf{f}}{(1+\mathrm{j}\eta)\,\omega_i^2}. \tag{19}$$

The second term at the right hand side of the equation is often called the *residual term*. As the next step, the static response $\mathbf{u}_0$ can be written as a modal expansion by substitution of $\omega = 0$ in equation (18) and taken into account that no structural damping occurs in the static situation

$$\mathbf{u}_0 = \sum_{i=1}^{m} \frac{\boldsymbol{\phi}_i\boldsymbol{\phi}_i^{\mathrm{T}}\mathbf{f}}{\omega_i^2} + \sum_{i=m+1}^{n} \frac{\boldsymbol{\phi}_i\boldsymbol{\phi}_i^{\mathrm{T}}\mathbf{f}}{\omega_i^2}. \tag{20}$$

With this result, equation (19) becomes:

$$\mathbf{u} \approx \sum_{i=1}^{m} \frac{\boldsymbol{\phi}_i\boldsymbol{\phi}_i^{\mathrm{T}}\mathbf{f}}{(1+\mathrm{j}\eta)\,\omega_i^2 - \omega^2} + \frac{\mathbf{u}_0}{(1+\mathrm{j}\eta)} - \sum_{i=1}^{m} \frac{\boldsymbol{\phi}_i\boldsymbol{\phi}_i^{\mathrm{T}}\mathbf{f}}{(1+\mathrm{j}\eta)\,\omega_i^2}. \tag{21}$$

This implies an extra static analysis when the residual mode is taken into account.

With the derived equations the response at different nodal locations of the receiver structure can be determined. The complete mobility matrix $\mathbf{Y}_r$ is composed (see equation (5)) by computation of the receiver velocities at all degrees of freedom that connect the mounts with the receiver structure for a unity excitation force $\mathbf{f}$ in each degree of freedom at each mount (described by the excitation force vector $\mathbf{f}$). In the same way mobility matrices for the positions of the vibrational sensors are calculated

$$\mathbf{v}_s = \mathbf{Y}_{rs}\mathbf{f}_r, \tag{22}$$

where $\mathbf{v}_s$ a vector with responses of vibration sensors at specified locations of the receiver structure and $\mathbf{Y}_{rs}$ the corresponding mobility matrix.

3 Sensor strategies

The dominant excitations of rotary machinery like engines and gearboxes in lightweight vehicles are mostly deterministic and characterized by the engine orders. The excitation is assumed to be harmonic and narrow band feedforward control strategies can be used to tackle the control problem. The reference signal used by the controller is in this case a tacho-signal measured at the engine. The controller uses the reference signal and drives the actuators in such a way that the cost function based on the sum of the squared amplitudes of the sensor responses [12] is minimized:

$$J = \mathbf{v}_s^{\mathrm{H}} \mathbf{v}_s = \sum_{i=1}^{N} |v_s(i)|^2, \tag{23}$$

where N the number of sensors and $(.)^{\mathrm{H}}$ the complex conjugate transpose. The sensor response can be written as a function of the disturbance force vector $\mathbf{f}_d$ and the actuator force vector $\mathbf{f}_a$ according to

$$J = \left(\mathbf{H}_p \mathbf{f}_d + \mathbf{H}_s \mathbf{f}_a\right)^{\mathrm{H}} \left(\mathbf{H}_p \mathbf{f}_d + \mathbf{H}_s \mathbf{f}_a\right), \tag{24}$$

where $\mathbf{H}_p$ the primary transfer function representing the transfer from the disturbance force to the sensor response and $\mathbf{H}_s$ the secondary transfer function representing the transfer from the actuator forces to the sensor response. The error criterion is written in the so-called Hermitian quadratic form, which in general is expressed as

$$J = \mathbf{f}_a^{\mathrm{H}} \mathbf{A} \mathbf{f}_a + \mathbf{f}_a^{\mathrm{H}} \mathbf{b} + \mathbf{b}^{\mathrm{H}} \mathbf{f}_a + c, \tag{25}$$

where

$$\mathbf{A} = \mathbf{H}_s^{\mathrm{H}} \mathbf{H}_s \tag{26}$$

$$\mathbf{b} = \mathbf{H}_s^{\mathrm{H}} \mathbf{H}_p \mathbf{f}_d \tag{27}$$

$$c = \mathbf{f}_d^{\mathrm{H}} \mathbf{H}_p^{\mathrm{H}} \mathbf{H}_p \mathbf{f}_d \tag{28}$$

The optimum actuator force that minimizes the quadratic error criterion is

$$\mathbf{f}_a^{\mathrm{opt}} = -\mathbf{A}^{-1} \mathbf{b} \tag{29}$$

and the corresponding minimum sensor response is

$$\mathbf{v}_s^{\mathrm{opt}} = c - \mathbf{b}^{\mathrm{H}} \mathbf{A}^{-1} \mathbf{b}. \tag{30}$$

3.1 Vibration sensors

In case of vibration isolation, vibrations sensors are placed at the receiver structure. The error criterion described by these sensors can also be written in the Hermitian quadratic form. The response of the vibration sensor set is written as

$$\mathbf{v}_s = \mathbf{Y}_{rs} \mathbf{f}_r, \tag{31}$$

where $\mathbf{Y}_{rs}$ is the mobility matrix from the receiver forces at the junctions to the sensors located at the receiver structure. The primary and secondary transfer functions are determined by equations (11) and (31) resulting in

$$\mathbf{H}_p = -\mathbf{Y}_{rs} \mathbf{T} \mathbf{H}_1 \qquad \mathbf{H}_s = -\mathbf{Y}_{rs} \mathbf{T} \mathbf{H}_2. \tag{32}$$

The optimum actuator force can now be calculated as described by equations (26) till (29).

3.2 Transmitted power

The transmitted power from the source to the receiver structure is a measure of the energy content of the complete receiver structure. For this reason, this quantity is an interesting error criterion for active isolation and is determined by

$$J = P_t = \frac{1}{2}\mathrm{Re}\left(\mathbf{f}_r^{\mathrm{H}}\mathbf{v}_r\right) = \frac{1}{4}\left(\mathbf{f}_r^{\mathrm{H}}\mathbf{v}_r + \mathbf{v}_r^{\mathrm{H}}\mathbf{f}_r\right), \tag{33}$$

where P_t the transmitted power. With the help of equations (9) and (11) the transmitted power is written in a Hermitian quadratic form with the coefficients (see equation (25)):

$$\mathbf{A} = \frac{1}{4}\left(\mathbf{H}_2^{\mathrm{H}}\mathbf{T}^{\mathrm{H}}\mathbf{Y}_r\mathbf{T}\mathbf{H}_2 + \mathbf{H}_2^{\mathrm{H}}\mathbf{T}^{\mathrm{H}}\mathbf{Y}_r^{\mathrm{H}}\mathbf{T}\mathbf{H}_2\right) \tag{34}$$

$$\mathbf{b} = \frac{1}{4}\left(\mathbf{H}_2^{\mathrm{H}}\mathbf{T}^{\mathrm{H}}\mathbf{Y}_r\mathbf{T}\mathbf{H}_1 + \mathbf{H}_2^{\mathrm{H}}\mathbf{T}^{\mathrm{H}}\mathbf{Y}_r^{\mathrm{H}}\mathbf{T}\mathbf{H}_1\right)\mathbf{f}_d \tag{35}$$

$$\mathbf{c} = \frac{1}{4}\mathbf{f}_d^{\mathrm{H}}\left(\mathbf{H}_1^{\mathrm{H}}\mathbf{T}^{\mathrm{H}}\mathbf{Y}_r\mathbf{T}\mathbf{H}_1 + \mathbf{H}_1^{\mathrm{H}}\mathbf{T}^{\mathrm{H}}\mathbf{Y}_r^{\mathrm{H}}\mathbf{T}\mathbf{H}_1\right)\mathbf{f}_d \tag{36}$$

3.3 Weighting of near-source sensors

In practice the transmitted power is difficult to measure and is ill-conditioned due to its sensitivity to phase errors [5]. Besides that, interface forces and velocities have to be measured simultaneously, both in three translational and in three angular directions, which is not very attractive. For this reason another sensor strategy is considered based on weighting near-source sensor signals with a measured transfer matrix.

A far-field sensor set is located e.g. in the accommodations of the ship (e.g. microphones) and a near-source sensor set is located near the engine. As the next step a weighting matrix between the two sensor sets is measured. In the real-life application only the near-source sensor set is applied and weighted by the weighting matrices which are determined in advance. The procedure how to implement such a weighting matrix will be explained. The dynamics of the total isolation system can be written in terms of one mobility matrix:

$$\begin{Bmatrix}\mathbf{v}_d\\ \mathbf{v}_a\\ \mathbf{v}_{ns}\\ \mathbf{v}_{fs}\\ \mathbf{v}_c\end{Bmatrix} = \begin{bmatrix}\mathbf{Y}_{dd} & \mathbf{Y}_{da} & \mathbf{Y}_{dns} & \mathbf{Y}_{dfs} & \mathbf{Y}_{dc}\\ \mathbf{Y}_{ad} & \mathbf{Y}_{aa} & \mathbf{Y}_{ans} & \mathbf{Y}_{afs} & \mathbf{Y}_{ac}\\ \mathbf{Y}_{nsd} & \mathbf{Y}_{nsa} & \mathbf{Y}_{nsns} & \mathbf{Y}_{nsfs} & \mathbf{Y}_{nsc}\\ \mathbf{Y}_{fsd} & \mathbf{Y}_{fsa} & \mathbf{Y}_{fsns} & \mathbf{Y}_{fsfs} & \mathbf{Y}_{fsc}\\ \mathbf{Y}_{cd} & \mathbf{Y}_{ca} & \mathbf{Y}_{cns} & \mathbf{Y}_{cfs} & \mathbf{Y}_{cc}\end{bmatrix}\begin{Bmatrix}\mathbf{f}_d\\ \mathbf{f}_a\\ \mathbf{f}_{ns}\\ \mathbf{f}_{fs}\\ \mathbf{f}_c\end{Bmatrix}, \tag{37}$$

where $\mathbf{v}_d$ and $\mathbf{f}_d$ the velocities and forces at the upper side locations of the mounting system, $\mathbf{v}_a$ and $\mathbf{f}_a$ the velocities and forces at the actuator positions, $\mathbf{v}_{ns}$ and $\mathbf{f}_{ns}$ the velocities and forces at the near-source sensor locations, $\mathbf{v}_{fs}$ and $\mathbf{f}_{fs}$ the velocities and forces at the far-field sensor locations and $\mathbf{v}_c$ and $\mathbf{f}_c$ the velocities and forces at the remaining part of the receiver structure. The corresponding partial mobilities are also depicted in the full receiver mobility matrix. When it is assumed that only disturbance forces act on top of the mounting system and actuator forces act at the connection points of the mounts with the receiver structure, the response at the two sensor sets can be written as:

$$\begin{Bmatrix}\mathbf{v}_{ns}\\ \mathbf{v}_{fs}\end{Bmatrix} = \begin{bmatrix}\mathbf{Y}_{nsd} & \mathbf{Y}_{nsa}\\ \mathbf{Y}_{fsd} & \mathbf{Y}_{fsa}\end{bmatrix}\begin{Bmatrix}\mathbf{f}_d\\ \mathbf{f}_a\end{Bmatrix}. \tag{38}$$

When the disturbance and actuator force vectors are combined, the following equations result:

$$\mathbf{v}_{ns} = \mathbf{Y}_{nsda}\mathbf{f}_{da}, \tag{39}$$

$$\mathbf{v}_{fs} = \mathbf{Y}_{fsda}\mathbf{f}_{da}. \tag{40}$$

With these two equations, the far-field sensor response can be written as function of the near-source sensor response according to

$$\mathbf{v}_{fs} = \mathbf{W}_v\mathbf{v}_{ns} = \mathbf{Y}_{fsda}\mathbf{Y}_{nsda}^{+}\mathbf{v}_{ns}, \tag{41}$$

where $\mathbf{W}_v$ a weighting matrix of the near-source sensor response and $(.)^+$ indicates the pseudo-inverse. Considering the pseudo-inverse of the mobility matrix $\mathbf{Y}_{nsda}$, the number of near-source sensors must be at least equal to the sum of the number of independent excitation forces (or the number of mounts time the number of degrees of freedom per mount) and actuators, else the pseudo-inverse of an ill-conditioned matrix is calculated.

However, considering equation (41) this type of weighting matrix is difficult to implement in a practical isolation system because the result depends on the actuator forces. These actuator forces are, generally speaking, varying with operational conditions and not easy to determine. For this reason it is necessary to define a weighting matrix which is valid for all excitations. With the help of equation (38) the far-field sensor response can be written as function of the near-source sensor response and actuator forces

$$\mathbf{v}_{fs} = \left(-\mathbf{Y}_{fsd}\mathbf{Y}_{nsd}^{+}\mathbf{Y}_{nsa} + \mathbf{Y}_{fsa}\right)\mathbf{f}_a + \mathbf{Y}_{fsd}\mathbf{Y}_{nsd}^{+}\mathbf{v}_{ns}. \tag{42}$$

The mobilities are determined like in equation (32) according to:

$$\mathbf{Y}_{nsd} = -\mathbf{Y}_{rns}\mathbf{T}\mathbf{H}_1 \qquad \mathbf{Y}_{fsd} = -\mathbf{Y}_{rfs}\mathbf{T}\mathbf{H}_1, \tag{43}$$

$$\mathbf{Y}_{nsa} = -\mathbf{Y}_{rns}\mathbf{T}\mathbf{H}_2 \qquad \mathbf{Y}_{fsa} = -\mathbf{Y}_{rfs}\mathbf{T}\mathbf{H}_2, \tag{44}$$

where $\mathbf{Y}_{rns}$ denotes the mobility matrix to the near-source sensor set of the receiver structure and $\mathbf{Y}_{rfs}$ denotes the mobility matrix to the far-field sensor set of the receiver structure. Considering equation (42) in more detail it is seen that the far-field sensor set, besides a weighting matrix multiplied with the near-source sensor response, depends on the actuator forces. However, for the SISO case (single input and single output, meaning one sensor and one actuator) with just one disturbance force component, it can easily been seen that the first term at the left-hand side of the equation reduces to zero. This implies that the actuator force influence is zero for all actuator forces. For a MIMO system (multiple sensors and actuators) with multiple independent disturbance directions this is not so straight-forward. Taken a closer look at the influence of the actuator force results in:

$$\underbrace{-\mathbf{Y}_{fsd}\,\underbrace{\mathbf{Y}_{nsd}^{+}\underbrace{\mathbf{Y}_{nsa}\mathbf{f}_a}_{\mathbf{v}_{nsa}}}_{\mathbf{f}_d^{eq}}}_{-\mathbf{v}_{fsa}} + \underbrace{\mathbf{Y}_{fsa}\mathbf{f}_a}_{\mathbf{v}_{fsa}} = \mathbf{0}, \tag{45}$$

where $\mathbf{v}_{nsa}$ denotes the near-source sensor response due to the actuator forces, $\mathbf{f}_d^{eq}$ denotes a disturbance force vector that is equivalent with the near-source sensor response due to the actuator forces and $\mathbf{v}_{fsa}$ denotes the far-field sensor response due to the actuator forces. However, equation (45) is only valid under certain circumstances, namely when $\mathbf{Y}_{nsd}$ is well conditioned for a reliable pseudo-inversion. The conditioning of this transfer matrix from the disturbance to the near-source sensor response depends on the number and position of the sensors. A necessary condition is that the number of near-source sensors must be at least equal to the number of disturbance forces, or in general at least equal to the number of mounts times 6. With the condition that the matrix $\mathbf{Y}_{nsd}$ is well conditioned, the far-field sensor response depends only on the near-field response according to

$$\mathbf{v}_{fs} = \mathbf{W}_v\mathbf{v}_{ns} = \mathbf{Y}_{fsd}\mathbf{Y}_{nsd}^{+}\mathbf{v}_{ns}\ . \tag{46}$$

3.3.1 Determination of weighting matrix $\mathbf{W}_v$

Generally speaking, a hybrid isolation system in a ship has to perform for a broad range of operational conditions like different running speeds and power. The excitation of the system, in the model characterized by the disturbance force vector $\mathbf{f}_d$, is different for these situations as well as the actuator forces determined by the controller. The weighting matrix for the near-source sensors must be valid for all these different disturbances caused by the engine. In practice, the weighting matrix is determined 'off-line', meaning that the influence of the different disturbances are measured under different operational conditions before implementation of

the active isolation system. In other words, a set of near-source sensors and a set of well-chosen far-field sensors are placed in the ship and the responses of both sensor sets are measured for j different operational conditions. The responses for each disturbance case of the near-source sensor set are stored in the matrix $\mathbf{V}_{ns}$ (number of near-source sensors $\times$ j) and the far-field sensor $\mathbf{V}_{fs}$ (number of far-field sensors $\times$ j), after which the weighting matrix can be determined as shown by Basten, v.d. Brink and Verheij [13] according to

$$\mathbf{W}_v = \mathbf{V}_{fs}\mathbf{V}_{ns}^{+}. \tag{47}$$

For a reliable prediction of the weighting matrix, the number of experiments must at least be equal to the number of near-source sensors and in fact must be at least be equal to the number of independent disturbance forces. The error criterion can now be determined according to

$$J = \mathbf{v}_{fs}^{\mathrm{H}}\mathbf{v}_{fs} = \mathbf{v}_{ns}^{\mathrm{H}}\mathbf{W}_v^{\mathrm{H}}\mathbf{W}_v\mathbf{v}_{ns} = \mathbf{v}_{ns}^{\mathrm{H}}\mathbf{W}\mathbf{v}_{ns}. \tag{48}$$

In this paper only numerical results are presented, and it is assumed that six independent forces and moments act on the top of each mount. The number of experiments must be at least equal to the number of mounts times six, and is simulated by choosing a random disturbance force vector.

4 Numerical simulations

The theory as described in the previous sections is implemented for a numerical model of a laboratory setup that is to a certain extent representative for a realistic carrier structure like a ship, see Figure 3. The two different types of near-source cost functions are considered and compared with each other: minimization of the transmitted power to the receiver structure and minimization of a weighted near-source sensor set. Two different weighted near-source sensor sets are considered.

4.1 Model

In Figure 3 a sketch of the laboratory setup used for experiments and numerical simulations is depicted. Different components are distinguished like a source, four mounts, and a receiver structure. The receiver structure consists of stiffened steel plates and beams and its overall dimensions are approximately 1.75 m $\times$ 0.9 m $\times$ 0.85 m and the plate thicknesses are 3 mm for the foundation plate and side plate and 2 mm for the radiation plate. The mounts are modeled as rigid pedestals for the simulations results presented.

Modal analysis shows that in the frequency range of 0 till 1000 Hz the receiver structure has about 250 eigenfrequencies. The mode shapes at low frequencies are characterized as global modes, while the modes at higher frequencies are characterized by local deformations of the structure. This behavior in combination with the relatively high modal density in the frequency range of interest makes this setup a representative test structure for research of hybrid vibration isolation systems in ships. The far field receiver response which is considered in the simulations is based on 25 equally distributed vibrations sensors on the radiation plate (see Figure 3).

4.2 Minimization of transmitted power

The minimization of transmitted power is an interesting error criterion for active isolation purposes, because it is directly related with the total energy content of the carrier structure. This implies that minimization of the transmitted power in practice results in minimization of the sum of the kinetic and potential energy. In Figure 4(a) the foundation plate is depicted with the disturbance forces (three unity forces in the translational directions and three unity moments in the rotational directions of each mount) and the actuator forces (one force in axial direction of each mount). In Figure 4(b) three responses are shown: the passive response of the far-field sensors, the active response of the far-field sensors when the transmitted power is minimized

and the minimum active response that can be obtained with minimization of the far-field sensor response itself. Minimization of the transmitted power results in an overall decrease of the far-field sensor response, but especially in the high frequency region the performance is much less than the optimal result.

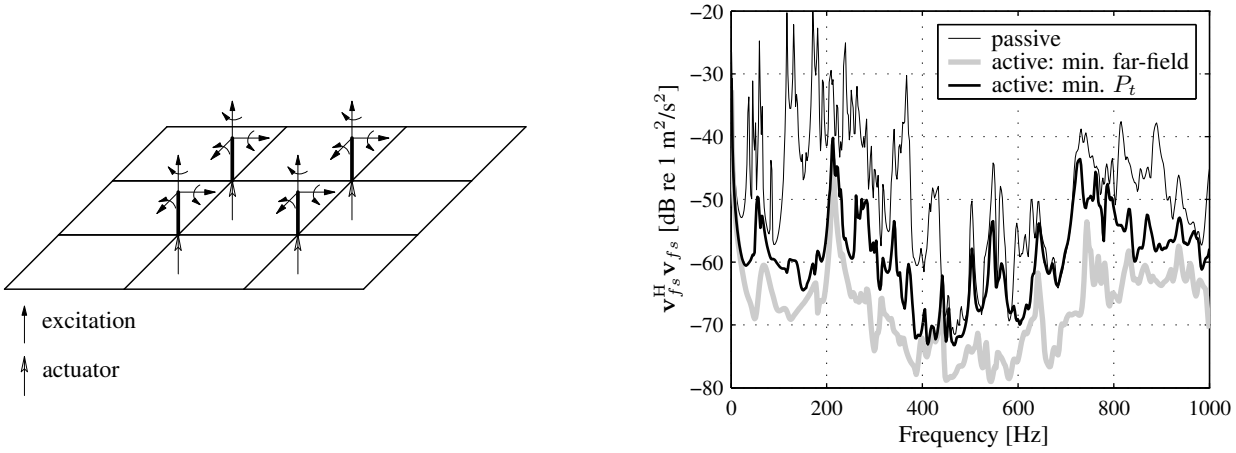

(a) (b)

Figure 4: Far-field sensor response with minimization of transmitted power.

4.3 Minimization weighted near-source error criteria

The other approach considered in this paper is based on weighting near-source sensor signals with a measured transfer matrix, describing the relation between near-source sensors and far-field sensors. The far-field sensor set is composed of the 25 vibration error sensors at the radiation plate as shown in Figure 3. First, the velocities at the connection points of the mounts with the receiver structure are considered as near-source sensor set, see Figure 5(a). In Figure 5(b) the far-field response is shown for the passive case, minimization of the unweighted near-source sensor response, the weighted near-source sensor response with minimization of the far-fields sensor response itself. When the near-source sensor response is minimized without a weighting matrix, poor reduction is obtained at the radiation plate. At some frequencies the response is even larger than the passive response. When a weighting matrix is determined as shown in equation (47), the obtained reduction is almost as large as in case of minimization of the far-field response. This is the goal of using the weighting matrix and improves the reduction considerably in comparison with the unweighted near-source error criterion.

The considered near-source error criterion with minimization of the translational and angular velocities of the receiver structure at the mount positions, is for practical reasons, not very attractive. A near-source sensor set is considered which consists only of normal velocity sensors at the foundation plate, see Figure 6(a). The weighting matrix for this sensor set can be determined with the same procedure and the results are shown in Figure 6(b). Active isolation based on minimization of the unweighted near-source sensor signals gives poor results. Weighting of the near-source sensor signal gives similar reductions as direct minimization of the far-field sensors.

4.4 Global response

Another important point of attention in case of active isolation is the global response of the receiver structure. Error criteria or cost functions based on a small part of the receiver structure in general results in a reduction at the error sensors itself, but may lead to an increase of the overall response. The overall measure is

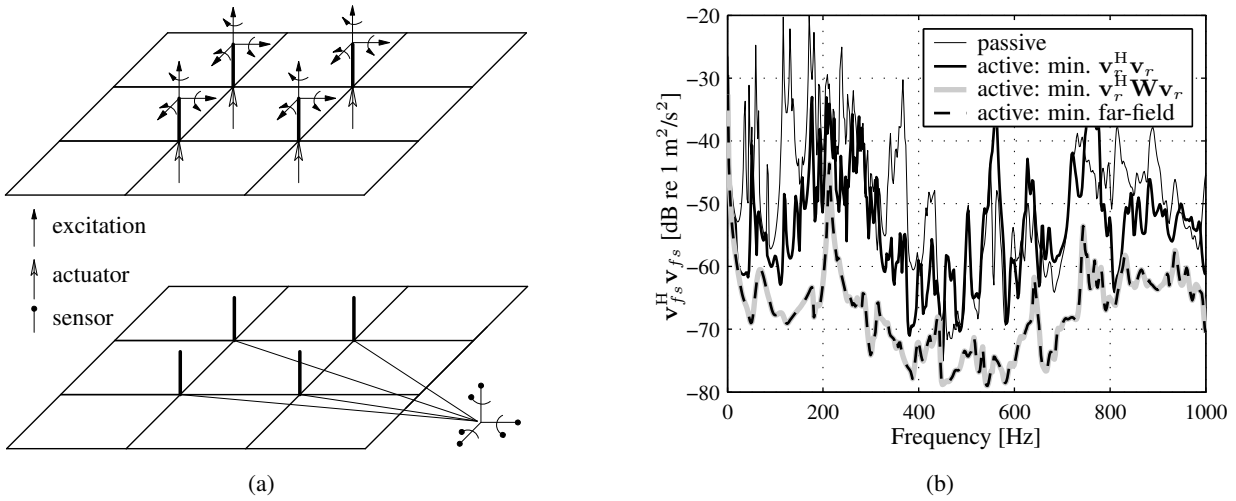

(a) (b)

Figure 5: Far-field sensor response for minimization of the velocities at the mount positions of the receiver (near-source sensor set 1).

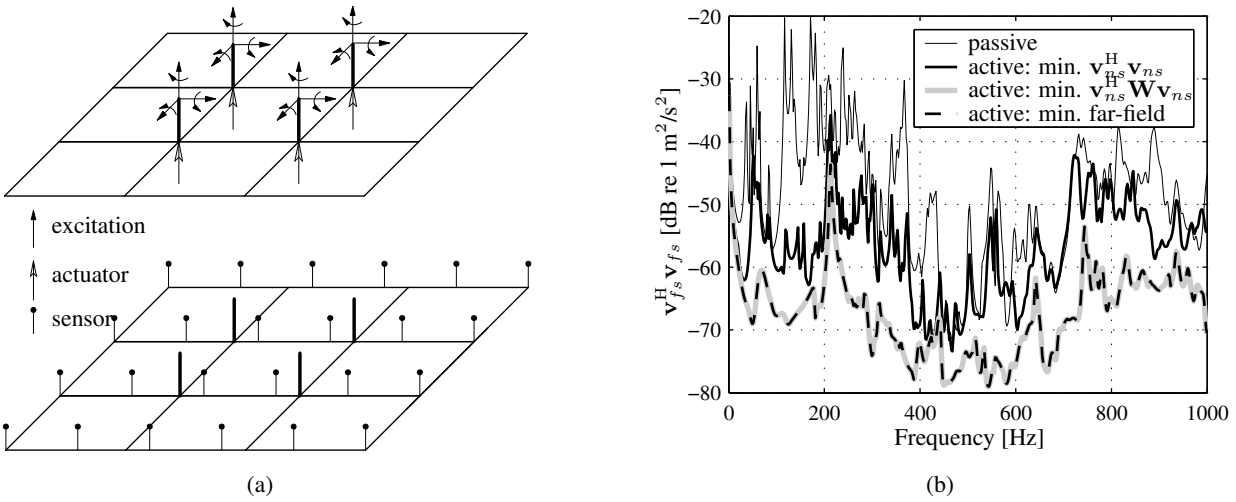

(a) (b)

Figure 6: Far-field sensor response for (weighted) minimization of a velocity sensor set at the foundation plate (near-source sensor set 2).

defined in this case as the quadratic summation of the velocities at all nodal points of the receiver structure: $J = \mathbf{v}_{tot}^{\mathrm{H}}\mathbf{v}_{tot}$. In Figure 7(a) the total response is shown for the passive situation, for minimization of the first considered (unweighted) near-source cost function (minimization of the connection velocities), for minimization of the second considered cost function (a set of normal velocities at the foundation plate) and for minimization of the total velocity response itself. Minimization of the receiver velocities at the connection points leads to a poor reduction of the overall response and at some frequencies the response is even larger compared to the passive response. It is seen that minimization of the near-source sensor set at the foundation plate results in a well overall reduction of the total response. In Figure 7(b) the total receiver response is depicted for minimization of the far-field sensor set situated at the radiation plate and for minimization of the transmitted power. As expected, minimization of the transmitted power results in almost the same reduction as minimization of the total velocity response itself, just a little bit less. The sum of the quadratic velocities at all nodal points of the receiver structure is a good indication of the kinetic energy of the system resulting in a good reduction. Minimization of the far-field sensor set gives poor reduction in terms of the overall

response.

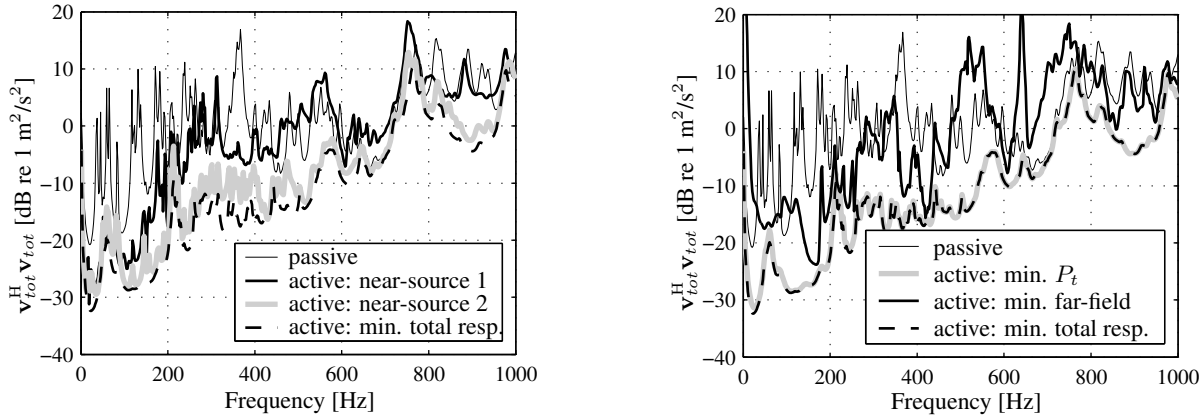

Figure 7: Influence of different cost functions on the total response of the receiver structure.

The total velocity response as shown in Figure 7(b) is not such a good measure to judge all considered error-criteria with respect to the far field response of the receiver structure. The response of the foundation plate is also taken into account in the total velocity response and has a relatively large contribution because it is situated near the source of excitation. So especially the performance of the near-source error criteria can be overestimated with respect to the total response of the receiver structure. For this reason only the responses of the side plate and the radiation plate are taken into account as global far field response of the receiver: $J = \mathbf{v}_{gl}^{\mathrm{H}}\mathbf{v}_{gl}$ (see Figure 3). The vector $\mathbf{v}_{gl}$ contains the velocities at all nodal points of the receiver plate and radiation plate. In Figure 8(a) the passive global response and the active global responses with

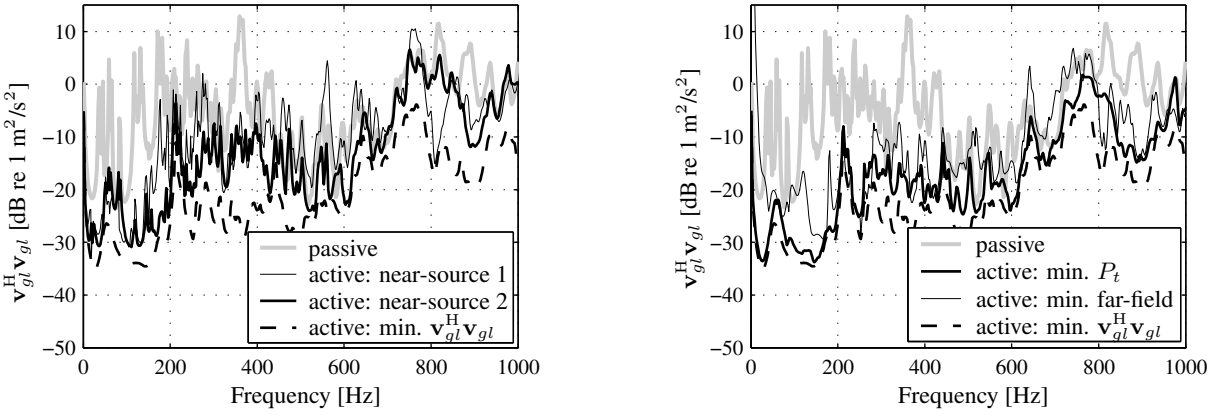

Figure 8: Influence of different cost functions on the global far field response (the side and radiation plate of the receiver structure).

minimization of the two near-source sensor sets and with minimization of the global response itself are shown. Both (unweighted) near-source sensor sets reduce only the response at the side and radiation plate at low frequencies, but at higher frequencies the reduction is limited or the active response even exceeds the passive response. In comparison with the total response, the reduction achieved with minimization of near-source sensor set 2 is poor, because mainly the response of the foundation plate is reduced.
In Figure 8(b) the global far field response is shown for minimization of the transmitted power and for

minimization of the far-field sensor set. Minimization of the transmitted power results in a reduction of the global response over the whole considered frequency range. Minimization of the far-field sensor set results in a reduction at the radiation plate, but the response of the side plate may increase. This means that the global response is not necessarily reduced with minimization of the far-field sensor set. However, the reduction of the global response is considerably larger than the total response, which means that the response of the source plate has a relatively large contribution in the active response for this sensor strategy. The active response based on the far-field sensor set results in a better global reduction than the responses based on the unweighted near-source sensor sets for the considered isolation system. The global and total responses of the weighted near-source sensor sets (weighted with the response based on the far-field sensor set) are not depicted because the same actuator forces are determined as in case of direct minimization of the far-field sensor set. This means that the total and global response with minimization of both weighted near-source sensor sets are similar to the total and global response with minimization of the far-field sensor set.

5 Discussion

For implementation of active isolation systems for noise reduction in ships, it is preferable to locate the sensors near the resiliently mounting system of the engine for reasons of simplicity, easier practical implementation and cost reduction. Two techniques of these so-called near-source error sensor strategies are analyzed: minimization of the transmitted power and weighting of a near-source sensor set in such a way that a far-field sensor response is minimized. The weighting matrix is obtained with off-line experiments. A theoretical model is presented to investigate the different error criteria with numerical simulations on a demonstrator model that is to a certain extent representative for a realistic application in terms of dynamical behavior.

It is shown that minimization of transmitted power leads to a reduction of the chosen far-field sensor set, although the performance is not so good as with minimization directly on the far-field sensor set. The advantage of minimization of transmitted power is that a global reduction is obtained, but it is known that this error criterion is very sensitive for measurement errors and it is hardly possible to apply this error strategy in practical isolation systems. For this reason the alternative near-source cost function is analyzed, based on weighting of a near-source sensor set. Weighting of a near-source sensor set leads to a very good performance at the far field sensors, that is comparable with direct minimization of the far-field sensor set. However, minimization of the specific far-field sensor set is no guarantee that a reduction of the overall vibration level is obtained, even an increase in comparison with the passive response is possible, so care must be taken in the choice of the far-field sensor set. Therefore, weighting strategies giving good global reductions have to be investigated in more detail.
Also the robustness of the weighting method has to be studied. Analysis using singular value decomposition of the weighting matrix showed that the structural transfer matrices are dominated by just a few singular values and corresponding singular vectors [13]. This can be used to determine a more robust weighting matrix. Also further investigation is necessary for an experimental procedure to measure the weighting matrix.

6 Acknowledgements

This research was carried out under the joint research program “Hybrid Isolation of Structure Borne Sound” from TNO TPD and the University of Twente.

References

[1] M. Winberg, S. Johansson, T.L. Lagö, *Control approaches for active noise and vibration control in a naval application*, *Proceedings of the Seventh International Congress on Sound and Vibration, Garmisch-Partenkirchen, Germany, 2000 July, pp. 27-30*.

[2] M. Winberg, S. Johansson, T.L. Lagö, *Active control of engine induced noise in a naval application*, *Proceedings of the Eight International Congress on Sound and Vibration, Hong Kong, China, 2001 July, pp. 2-6*.

[3] J. Pan, C.H. Hansen, J. Pan, *Active isolation of a vibration source from a thin beam using a single active mount*, Journal of Acoustical Society of America, Vol. 94, No. 3, 1993, pp. 1425-1434.

[4] P. Gardonio, S.J. Elliott, R.J. Pinnington, *Active isolation of structural vibration on a multiple-degree-of-freedom system, Part I: The Dynamics of the system*, Journal of Sound and Vibration, Vol. 207, No. 1, 1997, pp. 61-93.

[5] P. Gardonio, S.J. Elliott, R.J. Pinnington, *Active isolation of structural vibration on a multiple-degree-of-freedom system, Part II: Effectiveness of active control strategies*, Journal of Sound and Vibration, Vol. 207, No. 1, 1997, pp. 95-121.

[6] J.C. Snowdon, *Vibration isolation: Use and characterization*, Journal of the Acoustical Society of America, Vol. 66, No. 5, 1979, pp. 1245-1274.

[7] L. Kari, *Dynamic transfer stiffness measurements of vibration isolators in the audible frequency range*, Noise Control Engineering Journal, Vol. 49, No. 2, 2001, pp. 88-102.

[8] C.A.J. Beijers, A. de Boer, *Numerical modelling of rubber vibration isolators*, *Proceedings of the Tenth International Congress on Sound and Vibration, Stockholm, Sweden, 2003 July, pp. 805-812*.

[9] T.G.H. Basten, J.W. Verheij, *Actuator and sensor configurations in hybrid isolation of machinery vibration*, *Proceedings of the Tenth International Congress on Sound and Vibration, Stockholm, Sweden, 2003 July, pp. 149-156*.

[10] C.A.J. Beijers, A. de Boer, *Hybrid isolation of structure-borne sound*, *Proceedings of Active 2002, Southampton, UK, 2002 July, pp. 291-302*.

[11] R.R. Craig, *Structural dynamics: an introduction to computer methods*, Wiley, New York (1981).

[12] P.A. Nelson and S.J. Elliott, *Active control of sound*, Academic Press, New York (1992).

[13] T.G.H. Basten, D.R. van den Brink, J.W. Verheij, *Near-source costfunctions for hybrid isolation of structure-borne sound*, *Proceedings of the Eleventh International Congress on Sound and Vibration, St. Petersburg, Russia, 2004 July*.